Available online at www.sciencedirect.com

ScienceDirect

Physics Procedia 66 (2015) 95 – 104

Physics Procedia

C 23rd Conference on Application of Accelerators in Research and Industry, CAARI 2014

Artificially Structured Boundary as a Charged Particle Beam Deflector Shield

R. M. Hedlof and C. A. Ordonez*

Department of Physics, University of North Texas, Denton, Texas 76203, USA

Abstract

The possibility of using a planar artificially structured boundary as a charged particle beam deflector shield is studied via classical trajectory Monte Carlo simulation. The artificially structured boundary (ASB) is formed by a planar array of permanent disk magnets with like poles facing out and creates a spatially periodic magnetostatic field. A mono-energetic beam of charged particles is incident on the ASB, and the conditions under which particles penetrate through the array are determined.

Selection and peer-review under responsibility of the Organizing Committee of CAARI 2014

Keywords: Beam control; classical trajectory; Monte Carlo; simulation

1. Introduction

The manipulation and confinement of charged particles is important in many areas of current research. An example is the effort to synthesize and study antihydrogen.[1–4] Antihydrogen with very low temperature is highly desirable for gravity experiments.[5–8] Antihydrogen has been produced by mixing antiproton and positron plasmas in nested Penning traps, however various issues may need to be addressed before this method will yield antiatoms with temperatures suitable for precision spectroscopy or gravity experiments.[1,9]

* Corresponding author.
E-mail address: cao@unt.edu

Selection and peer-review under responsibility of the Organizing Committee of CAARI 2014
doi:10.1016/j.phpro.2015.05.014

An artificially structured boundary (ASB) creates a spatially periodic field, such that the spatial period of the field is much smaller than the dimensions of a source of charged particles that is near the boundary. Various configurations of electrodes and magnets can create an ASB, and previous work involving charged particle and plasma interactions with several of these configurations may be found in Refs. [10-12]. The work presented here is motivated by the possibility of developing an alternative scheme, using an artificially structured boundary, to confine and manipulate antimatter plasmas and beams for antihydrogen production.

In the present work, a planar array of 25 permanent disk magnets with like-poles facing outward is used to create an ASB with a spatially periodic magnetostatic field. The spatial period of the field is considered to be much smaller than the dimensions of an incident beam of charged particles. As a result, the effective range of the magnetic field is smaller than the beam radius and the particles are effectively un-magnetized unless located relatively close to the ASB. The disk magnets are approximated as infinitesimally thin circular wire loops, each carrying current in the counter-clockwise sense as viewed from the positive z direction. A Cartesian coordinate system is defined such that the array lies in the x-y plane with the axis of symmetry of the middle loop along the z axis. A conceptual illustration of the configuration is shown in Fig. 1a, and a magnified view of the innermost nine current loops is shown in Fig. 1b. The current loops are arranged in a grid pattern, where the distance between the centers of adjacent loops in both the x and y directions is S. Arranged in such a manner, the array of loops produces a magnetostatic field that is periodic in the x and y directions, with spatial period S. A classical trajectory Monte Carlo study is presented that is used to determine the conditions under which charged particles penetrate through the ASB.

(a) (b)

Fig. 1: (a) A conceptual illustration of the ASB. (b) A magnified view of the inner nine current loops.

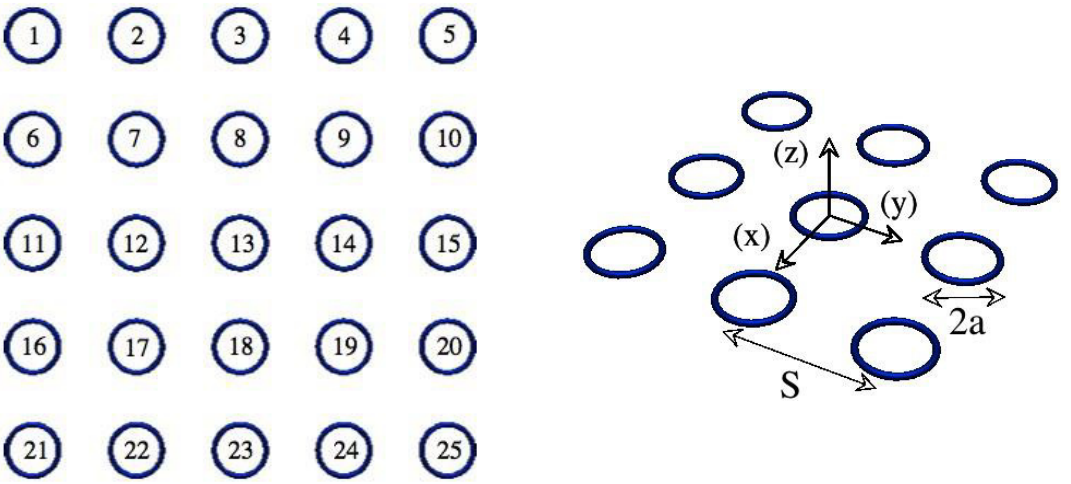

2. Classical Trajectory Monte Carlo Simulation

2.1. Magnetic Field of a Current Loop

The components of the magnetic field due to a single current loop of radius a, centered about the origin of a cylindrical coordinate system, and lying in the $z = 0$ plane are

$$B_r = \frac{B_m}{\pi}\eta_1(r,z)[\kappa_1(r,z)E(m_a) - K(m_a)],$$

$$B_z = \frac{B_m}{\pi}\eta_2(r,z)[\kappa_2(r,z)E(m_a) + K(m_a)]. \quad (1)$$

Here, $B_m = \mu_0 I/(2a)$ is the magnitude of the field at the origin, I is the current in the loop, μ_0 is the permeability of free space, $m_a = 4ar/[(r+a)^2 + z^2]$ and the coefficients η_1, η_2, κ_1, and κ_2 are, respectively,

$$\eta_1(r,z) = \frac{az}{r\sqrt{(a+r)^2+z^2}},$$

$$\eta_2(r,z) = \frac{a}{\sqrt{(a+r)^2+z^2}},$$

$$\kappa_1 = \frac{a^2+r^2+z^2}{(a-r)^2+z^2},$$

$$\kappa_2 = \frac{a^2-(r^2+z^2)}{(a-r)^2+z^2}. \quad (2)$$

Also, the complete elliptical integrals of the first and second kind, $K(m_a)$ and $E(m_a)$, are given by

$$K(m_a) = \int_0^{\frac{\pi}{2}} (1 - m_a \sin^2(\theta))^{-\frac{1}{2}}\, d\theta,$$

$$E(m_a) = \int_0^{\frac{\pi}{2}} (1 - m_a \sin^2(\theta))^{\frac{1}{2}}\, d\theta. \quad (3)$$

2.2. Normalization

All parameters used in the simulation are normalized such that they are dimensionless quantities. Normalized parameters are denoted by the same symbol as their un-normalized counterparts, but with the subscript *n* attached. The parameters used for normalization are the spatial period of the magnetic field S, the kinetic energy of the particle K, the particle's charge q, and the particle's mass m. The normalized value for each of these parameters is unity, $S_n = K_n = q_n = m_n = 1$. The particle's normalized position, velocity, and acceleration are then $\boldsymbol{r}_n = \boldsymbol{r}/S$, $\boldsymbol{v}_n = \boldsymbol{v}\sqrt{m/K}$ and $\boldsymbol{a}_n = \boldsymbol{a}mS/K$, respectively. The normalized time and magnetic field are given by $t_n = tS^{-1}\sqrt{K/m}$ and $\boldsymbol{B}_n = \boldsymbol{B}qS/\sqrt{mK}$. A normalized version of Newton's second law is obtained by solving these relations for the un-normalized parameters and substituting into $m\boldsymbol{a} = q\boldsymbol{v} \times \boldsymbol{B}$, yielding $\boldsymbol{a}_n = \boldsymbol{v}_n \times \boldsymbol{B}_n$.

The cyclotron radius r_c of a particle with kinetic energy *K* and moving in circular motion in a uniform magnetic field of magnitude *B* is given by $r_c = \sqrt{2mK}/|q|B$. In the case where the magnitude of the field is equal to that at the center of a single current loop (i.e., $B = B_m$), the magnitude of the normalized magnetic field may be written in terms of the cyclotron radius as

$$B_{mn} = sgn(q)\frac{\sqrt{2}}{r_{cn}}. \quad (4)$$

Here, $sgn(q) = q/|q|$ and $r_{cn} = r_c/S$. Substitution of Eq. (4) into Eq. (1) and writing the field in terms of normalized parameters yields the normalized magnetic field due to a single current loop

$$B_{rn} = \frac{sgn(q)\sqrt{2}}{\pi r_{cn}}\eta_{1n}(r_n,z_n)[\kappa_{1n}(r_n,z_n)E(m_a) - K(m_a)],$$

$$B_{zn} = \frac{sgn(q)\sqrt{2}}{\pi r_{cn}}\eta_{2n}(r_n,z_n)[\kappa_{2n}(r_n,z_n)E(m_a) + K(m_a)], \quad (5)$$

where the normalized coefficients η_{1n}, η_{2n}, κ_{1n}, and κ_{2n} are

$$\eta_{1n}(r_n, z_n) = \frac{a_n z_n}{r_n \sqrt{(a_n + r_n)^2 + {z_n}^2}},$$

$$\eta_{2n}(r_n, z_n) = \frac{a_n}{\sqrt{(a_n+r_n)^2+{z_n}^2}},$$

$$\kappa_{1n}(r_n, z_n) = \frac{a_n^2+r_n^2+z_n^2}{(a_n-r_n)^2+z_n^2},$$

$$\kappa_{2n}(r_n, z_n) = \frac{a_n^2-(r_n^2+z_n^2)}{(a_n-r_n)^2+z_n^2}. \quad (6)$$

2.3. Field Due to an Array of Loops

A Cartesian coordinate system is defined such that the origin lies at the center of the loop in the third row and third column as shown in Fig. 1b. The loops are numerically labelled by their position in the array, from left to right, top to bottom as shown in Fig. 1a. For example, row one contains loops 1-5, row two contains loops 6-10, row three contains loops 11-15, and so on. Therefore, the normalized magnetic field due to loop 13 is given by Eq. (5). To compute the field due to the entire array, it is convenient to first express Eq. (5) in Cartesian coordinates. Letting $r_n = \sqrt{x_n^2 + y_n^2}$ in Eq. (5), the components of the magnetic field produced by loop 13 may be written as

$$B_{xn,13}(x_n, y_n, z_n) = \frac{x_n B_{rn,13}}{\sqrt{x_n^2 + y_n^2}},$$

$$B_{yn,13}(x_n, y_n, z_n) = \frac{y_n B_{rn,13}}{\sqrt{x_n^2 + y_n^2}},$$

$$B_{zn,13}(x_n, y_n, z_n) = \frac{sgn(q)\sqrt{2}}{\pi r_{cn}} \eta_{2n}(x_n, y_n, z_n)[\kappa_{2n}(x_n, y_n, z_n)E(m_a) + K(m_a)]. \quad (7)$$

The field due to the *i*th current loop lying in the *x*-*y* plane and with center of mass coordinates ($x_{cmn,i}$, $y_{cmn,i}$) is then given by

$$B_{xn,i} = B_{xn,13}(x_n - x_{cmn,i}, y_n - y_{cmn,i}, z_n),$$

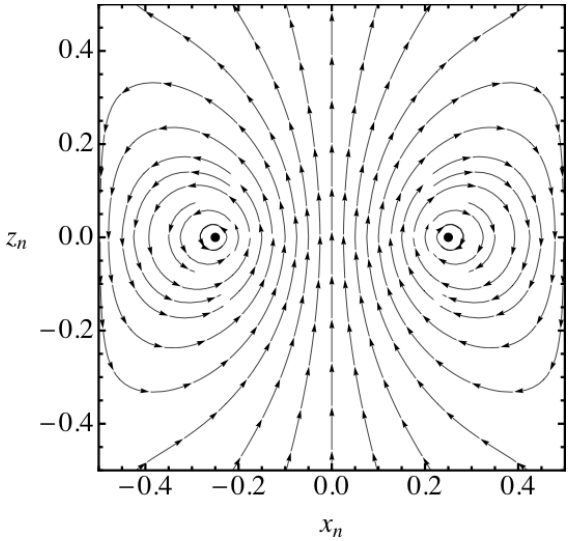

Fig. 2: Magnetic field lines in the x-z plane for one spatial period.

$$B_{yn,i} = B_{yn,13}\left(x_n - x_{cmn,i}, y_n - y_{cmn,i}, z_n\right),$$

$$B_{zn,i} = B_{zn,13}(x_n - x_{cmn,i}, y_n - y_{cmn,i}, z_n). \quad (8)$$

The field created by the array of loops is given by the superposition of the fields of each individual loop:

$$\boldsymbol{B}_n(x_n, y_n, z_n) = \sum_{i=1}^{25} \boldsymbol{B}_{n,i}\,(x_n, y_n, z_n). \quad (9)$$

A plot of the magnetic field lines for one spatial period in the *x-z* plane is shown in Fig. 2. The black dots in Fig. 2 represent the points where current loop 13 intersects the $y = 0$ plane. In the limit where the number of loops approaches infinity, or equivalently the array extends across the entire $z_n = 0$ plane, the magnetic field becomes spatially periodic in the x_n and y_n directions with spatial period S_n. As shown in Fig. 3, the magnitude $B_n = |\boldsymbol{B}_n|$ of the magnetic field decreases rapidly over a few spatial periods from the $z_n = 0$ plane in the $\widehat{\boldsymbol{k}}$ direction. The parameters used to generate Figs. 2 and 3 are $a_n = S_n/4$, $r_{cn} = 0.05$, and $sgn(q) = +1$.

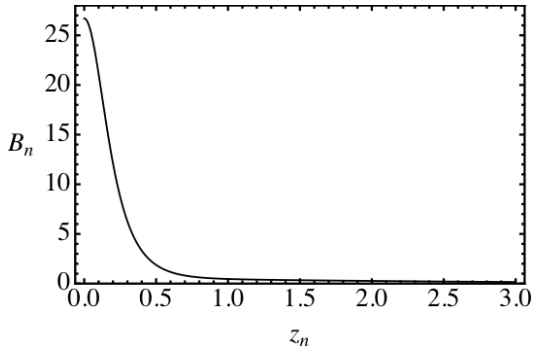

Fig. 3: The magnitude of the normalized magnetic field as a function of z_n, evaluated at $x_n = y_n = 0$ along the *z* axis.

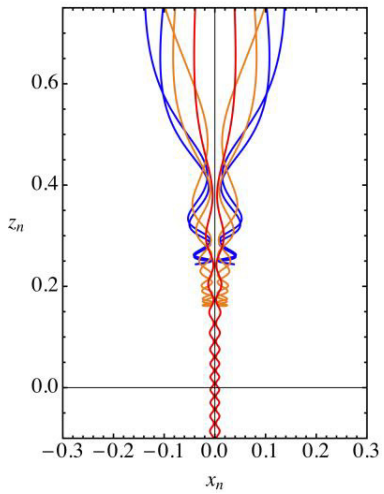

Fig. 4: Parametric plots in the *x*-*z* plane of the trajectories of six particles, two transmitted (red) and four reflected (two orange and two blue).

2.4. Simulation

A 3-D integration of each simulated particle's trajectory is carried out, with some initial phase space coordinates sampled randomly as is common in Monte Carlo simulations. Each particle's trajectory begins at normalized time $t_n = 0$. The initial coordinates for each particle (x_{0n}, y_{0n}) are considered to be equally likely to be located anywhere within a square of normalized side length $S_n = 1$ that is centered about the origin and has horizontal and vertical sides that are parallel with the x_n and y_n axes, respectively. The initial z_n coordinate of the particle is chosen sufficiently large such that the effect of the magnetic field is negligible, initially. The sampling expressions used for the initial Cartesian coordinates of each particle are

$$x_{0n} = R_x \frac{S_n}{2},$$

$$y_{0n} = R_y \frac{S_n}{2},$$

$$z_{0n} = 5. \qquad (10)$$

Here, R_x and R_y are random real numbers equally likely to have any value between −1 and 1. The simulated particles are mono-energetic, each with normalized kinetic energy $K_n = \frac{m_n v_n^2}{2} = 1$ and normalized speed $v_{0n} = \sqrt{2}$. The beam of particles is considered to be incident normally on the array of loops, and the initial velocity for each particle is:

$$\boldsymbol{v}_{0n} = -\sqrt{2}\hat{\boldsymbol{k}}. \qquad (11)$$

The normalized equations of motion are:

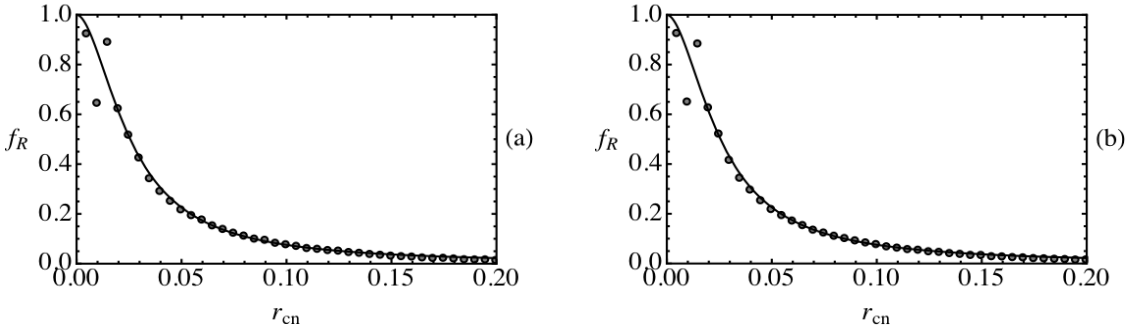

Fig. 5: The effect of varying the cyclotron radius for (a) positively charged particles and (b) negatively charged particles.

$$x_n''(t_n) = y_n'(t_n)B_{zn}(x_n, y_n, z_n) - z_n'(t_n)B_{yn}(x_n, y_n, z_n),$$

$$y_n''(t_n) = z_n'(t_n)B_{xn}(x_n, y_n, z_n) - x_n'(t_n)B_{zn}(x_n, y_n, z_n),$$

$$z_n''(t_n) = x_n'(t_n)B_{yn}(x_n, y_n, z_n) - y_n'(t_n)B_{xn}(x_n, y_n, z_n). \quad (12)$$

The equations of motion are solved numerically to simulate single particle trajectories. If the particle passes through the $z_n = 2$ plane and has a positive velocity in the z direction, the particle is considered to be reflected by the array. If the particle passes through the $z_n = 0$ plane, it is considered to be transmitted through the array. In the case where the array spans the entire $z_n = 0$ plane, all particles would be either transmitted or reflected. However, for the case where only 25 loops are present, it is possible for the particles to travel around the array. In the present work, particles reaching any of the $|x_n| = 2S_n$ or $|y_n| = 2S_n$ planes prior to reaching the $z_n = 0$ or $z_n = 2$ planes are considered to be "lost." Figure (4) shows the parametric plots, projected into the *x*-*z* plane, of the trajectories of six particles with initial coordinates along the $y_n = 0$ line in the $z_n = 5$ plane. The two red trajectories correspond to particles with initial coordinates $x_{0n} = \pm 0.1$, the two orange trajectories correspond to particles with initial coordinates $x_{0n} = \pm 0.2$, and the two blue trajectories correspond to particles with initial coordinates $x_{0n} = \pm 0.26$. Parameter values used to generate Fig. (4) were $sgn(q) = +1$, $a_n = S_n/4$, and $r_{cn} = 0.005$.

A study was carried out to determine how effective the array was in reflecting both positively and negatively charged particles for various values of normalized cyclotron radius. Let N_p, f_R, and f_L denote the number of simulated particles, the average fraction of those particles that were reflected by the array, and the fraction of particles that are lost, respectively. Each simulation run (e.g., with a given set of parameter values for N_p, $sgn(q)$, a_n, and r_{cn}) provides a single value for f_R. Ten (10) runs are carried out for each set of parameter values and the average fraction f_R is recorded. Figures 5a and 5b show the dependence of the fraction of reflected particles as a function of cyclotron radius for positive and negative particles, respectively, when the parameter values $N_p = 2,000$, $sgn(q) = \pm 1$, and $a_n = S_n/4 = 1/4$ are held constant. A fit of the classical trajectory Monte Carlo simulation results yields the expression:

$$f_R = \frac{1}{1+\lambda r_{cn}^{\gamma}}, \quad (13)$$

where $\lambda = 837.104$ and $\gamma = 1.83459$. The grey circles in Figures 5a and 5b represent the data gathered from the simulation, and the solid black line is the graph of Eq. (13). Aside from $r_{cn} = 0.01$ and $r_{cn} = 0.015$, for $0.005 \leq r_{cn} \leq 0.135$ Eq. (13) predicts the fraction of reflected particles to within 9% of the simulated results for both signs of charge.

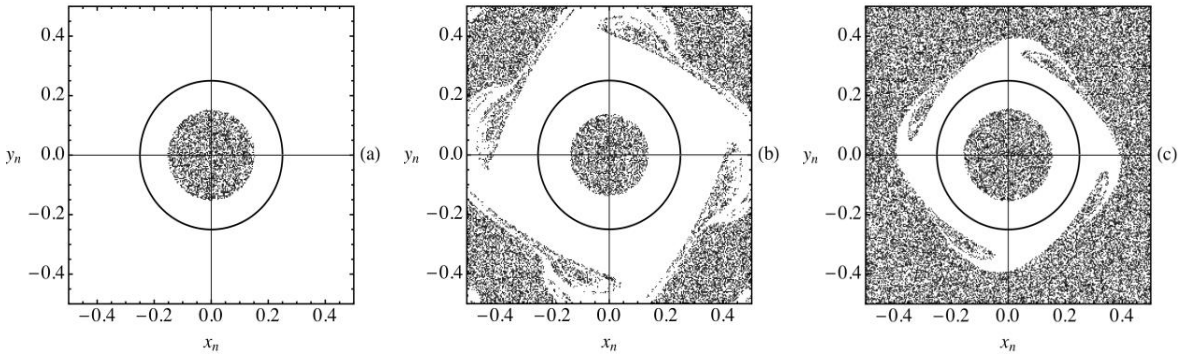

Fig. 6: Initial coordinates (x_{0n}, y_{0n}) of particles that were transmitted through the ASB for (a.) $r_{cn} = 0.005$, (b.) $r_{cn} = 0.025$, and (c.) $r_{cn} = 0.045$.

It is evident from Fig. 5 that the ASB is equally capable of reflecting particles of both signs of charge. In fact, the results for positively and negatively charged particles differ by no more than 11.7% at each data point. It should be noted that for certain values of r_{cn}, the fraction of lost particles was found to be as high as 9.2%. However, when they reached the $|x_n| = 2S_n$ or $|y_n| = 2S_n$ planes 8.67% had velocities in the positive z_n direction, while only 0.53% had velocities in the negative z_n direction. The particles with positive velocities in the z_n direction may correspond to trajectories that would be reflected if the array did in fact cover the entire $z_n = 0$ plane. Thus, the fraction of reflected particles may be slightly higher for certain values of r_{cn} than is shown in Figs. 5a and 5b.

In addition, the simulation was used to determine the location of weak points where particles are transmitted through the array. If a particle is transmitted, it's initial coordinates, as well as the particle's coordinates when it passes through the $z_n = 0$ plane are recorded. Each point in Figs. 6a-c represents the initial coordinates (x_{0n}, y_{0n}) of particles that were transmitted through the array. Alternatively, each of the points in Figs. 7a-c represents the coordinates (x_n, y_n) of these particles as they pass through the $z_n = 0$ plane. The black circles in figs. 6 and 7 represent the locations of the current loops. To generate the results in Fig. 6 and 7, the parameter values $N_p = 50,000$, $sgn(q) = +1$, and $a_n = 1/4$ were held constant, while the values used for the normalized cyclotron radius were: a.) $r_{cn} = 0.005$, b.) $r_{cn} = 0.025$, and c.) $r_{cn} = 0.045$. The number of particles that were transmitted through the ASB in Figs. 6 and 7 were: a.) 3, 666, b.) 19, 264, and c.) 33, 884. In Figs. 6a-c, all particles that had initial coordinates within a circle of normalized radius 0.152 were transmitted.

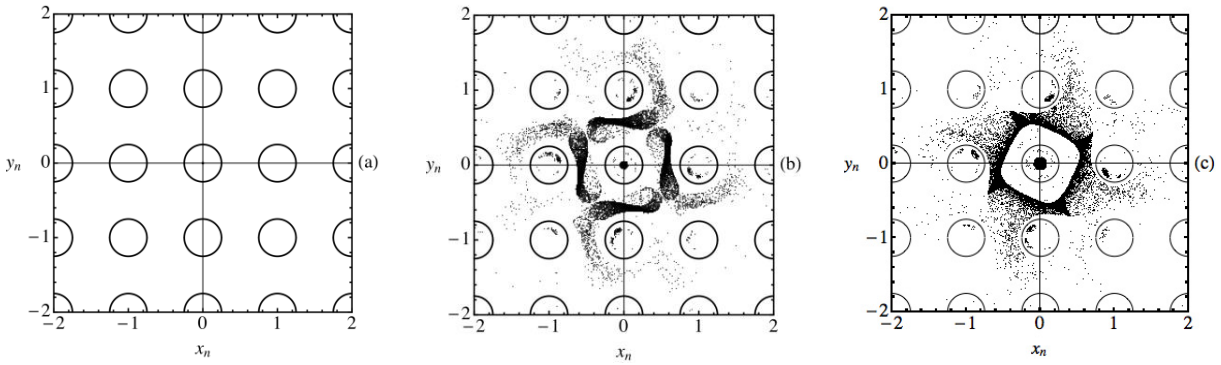

Fig. 7: Coordinates of transmitted particles as they cross the $z_n = 0$ plane for (a.) $r_{cn} = 0.005$, (b.) $r_{cn} = 0.025$, and (c.) $r_{cn} = 0.045$.

3. Discussion and Concluding Remarks

It should be noted that the apparatus envisioned would in fact be constructed using permanent disk magnets. As such, the constrained range of surface field strengths available in real magnets imposes limitations on the capability of the ASB to deflect high energy and heavy particles. To get an indication of these limitations, it is useful to write Eq. (13) in terms of un-normalized parameters. Taking the field strength B_m at the center of a current loop as a rough estimate of the surface field strength of a disk magnet, using Eq. (4), and noting that $B_{mn} = B_m qS/\sqrt{mK}$, Eq. (13) becomes

$$f_R = \frac{1}{1+\lambda\left[\sqrt{2mK}/(|q|SB_m)\right]^\gamma}. \qquad (14)$$

For example, if we have 300 eV electrons incident on an array of disk magnets, all with surface field strengths $B_m = 1$ T and $S = 1$ cm, the model predicts that 93.7% of the beam would be reflected. However, if a beam of 300 eV protons were incident on the same array only 1.5% would be reflected. This behaviour is easily seen qualitatively from Eq. (14). As the mass *m* or kinetic energy *K* increase, the denominator becomes larger, causing the predicted fraction of reflected particles to decrease. In current antihydrogen production experiments, the temperature of the positron and antiproton plasmas are typically less than 10 meV for both species; well within the range of energies the ASB can effectively reflect both species.

The configuration presented in this work creates a spatially periodic magnetostatic field that is short in range, only affecting the motion of charged particles that are within a distance of a few spatial periods of the array. In addition, the array reflects charged particles of either sign equally well. However, even for small values of normalized cyclotron radius, or equivalently, large magnetic field strengths there is some transmission of particles through the ASB. The regions where particles penetrate through the array have been identified, and if electrostatic plugging is introduced in these regions, it may be possible to achieve full reflection of all incident particles. However, further work is required to determine this for certain.

A classical trajectory Monte Carlo simulation has been used to determine the conditions under which the ASB deflects charged particles. A fit expression has been found for the fraction of particles that will be reflected by the ASB for a range of cyclotron radii. The fit can be used to predict the number of particles that will be reflected by the array of magnets forming the ASB.

ACKNOWLEDGEMENTS

The authors would like to thank R. Phillips and R. Lane for help with high performance computing. Computational resources were provided by UNT's High Performance Computing Services, a project of Academic Computing and User Services division of the University Information Technology with additional support from UNT Office of Research and Economic Development. This material is based upon work supported by the Department of Energy under Grant No. DE-FG02-06ER54883 and by the National Science Foundation under Grant No. PHY-1202428.

References:

1. G. B. Andresen, M. D. Ashkezari, M. Baquero-Ruiz, W. Bertsche, P. D. Bowe, E. Butler, C. L. Cesar, S. Chapman, M. Charlton, A. Deller, S. Eriksson, J. Fajans, T. Friesen, M. C. Fujiwara, D. R. Gill, A. Gutierrez, J. S. Hangst, W. N. Hardy, M. E. Hayden, A. J. Humphries, R. Hydomako, M. J. Jenkins, S. Jonsell, L. V. Jorgensen, L. Kurchaninov, N. Madsen, S. Menary, P. Nolan, K. Olchanski, A. Olin, A. Povilus, P. Pusa, F. Robicheaux, E. Sarid, S. Seif el Nasr, D. M. Silveira, C. So, J. W. Storey, R. I. Thompson, D. P. van der Werf, J. S. Wurtele, and Y. Yamazaki, Nature (London) **468**, 673 (2010).
2. G. Gabrielse, N. S. Bowden, P. Oxley, A. Speck, C. H. Storry, J. N. Tan, M. Wessels, D. Grzonka, W. Oelert, G. Schepers, T. Sefzick, J. Walz, H. Pittner, T. W. Hansch, and E. A. Hessels, Physical Review Letters **89**, 213401 (2002).
3. N. Kuroda, S. Ulmer, D. Murtagh, S. Van Gorp, Y. Nagata, M. Diermaier, S. Federmann, M. Leali, C. Malbrunot, V. Mascagna, O. Massiczek, K. Michishio, T. Mizutani, A. Mohri, H. Nagahama, M. Ohtsuka, B. Radics, S. Sakurai, C. Sauerzopf, K. Suzuki, M.

Tajima, H. Torii, L. Venturelli, B. Wunschek, J. Zmeskal, N. Zurlo, H. Higaki, Y. Kanai, E. Lodi Rizzini, Y. Nagashima, Y. Matsuda, E. Widmann and Y. Yamazaki, Nature Communications **5**, 3089 (2014).

4. D. Fabris, A. Belov, G. Bonomi, I. Boscolo, N. Brambilla, R. Brusa, V. Byakov, L. Cabaret, C. Canali, C. Carraro, F. Castelli, S. Cialdi, D. Comparat, G. Consolati, L. Dassa, N. Djourelov, M. Doser, G. Drobychev, A. Dudarev, A. Dupasquier, R. Ferragut, G. Ferrari, A. Fischer, P. Folegati, A. Fontana, L. Formaro, M. Lunardon, A. Gervasini, M. Giammarchi, S. Gninenko, R. Heyne, S. Hogan, L. Jorgensen, A. Kellerbauer, D. Krasnicky, V. Lagomarsino, F. Leveraro, G. Manuzio, S. Mariazzi, V. Matveev, F. Merkt, S. Moretto, C. Morhard, G. Nebbia, P. Nedelec, M. Oberthaler, D. Perini, V. Petracek, M. Prevedelli, I. Al-Qaradawi, F. Quasso, C. Riccardi, O. Rohne, S. Pesente, A. Rotondi, M. Spacek, S. Stapnes, D. Sillou, S. Stepanov, H. Stroke, G. Testera, G. Tino, D. Trezzi, A. Turbabin, R. Vaccarone, A. Vairo, G. Viesti, H. Walters, U. Warring, S. Zavatarelli, A. Zenoni and D. Zvezhinskij, Nuclear Physics A **834**, 751c (2010).
5. P. Perez and Y. Sacquin, Classical and Quantum Gravity **29**, 184008 (2012).
6. C. A. Ordonez and R. M. Hedlof, AIP Advances **2**, 012176 (2012).
7. R.M. Hedlof and C. A. Ordonez, Application of Accelerators in Research and Industry, AIP Conference Proceedings **1525** (2013) 102-105.
8. J. R. Rocha, R. M. Hedlof and C. A. Ordonez, AIP Advances **3**, 102129 (2013).
9. C. A. Ordonez and D. L. Weathers, Physics of Plasmas **15**, 083504 (2008).
10. C. A. Ordonez, Physics of Plasmas **15**, 114507 (2008).
11. C. A. Ordonez, Journal of Applied Physics **106**, 024905 (2009).
12. J. L. Pacheco, C. A. Ordonez and D. L. Weathers, Physics of Plasmas **19**, 102510 (2012).